

## Neutron-scattering study on phase transitions of $\text{CsPbCl}_3$ <sup>†</sup>

Y. Fujii\* and S. Hoshino

*Institute for Solid State Physics, The University of Tokyo, Minato-ku, Tokyo 106, Japan*

Y. Yamada

*College of General Education, Osaka University, Toyonaka, Osaka 560, Japan*

G. Shirane

*Brookhaven National Laboratory,<sup>‡</sup> Upton, New York 11973*

(Received 20 December 1973)

Neutron-scattering experiments have elucidated the mechanism of the successive phase transitions of  $\text{CsPbCl}_3$  at 47, 42, and 37°C. These phase transitions are basically associated with the condensation of rotational modes of  $\text{PbCl}_6$  octahedra around the three principal axes. The phase transition at 47°C is caused by the condensation of the nondegenerate  $M_3$  phonon mode at the zone boundary along the [110] direction of the cubic lattice. The axis of rotation of the  $\text{PbCl}_6$  octahedra is along the [001] axis. The second phase transition at 42°C is associated with the condensation of one of doubly degenerate modes  $Z_3^5$  and  $Z_3^7$  at the zone boundary along the [001] direction of the tetragonal lattice, which are derived from the triply degenerate  $R_{25}$  mode in the cubic phase. The direction of the rotation axis is along the [100] axis when we assign  $Z_3^5$  as the condensing mode. The third phase transition at 37°C is caused by the condensation of the remaining  $Z_3^7$  mode. The crystal systems and the space groups of three low-temperature phases were determined from the eigenvectors of the condensing modes as tetragonal  $D_{2h}^5$ , orthorhombic  $D_{2h}^{17}$ , and monoclinic  $C_{2h}^2$  in the sequence of decreasing temperature. These are consistent with the previous experimental results on nuclear-quadrupole-resonance spectra of  $\text{Cl}^-$  ion. A phenomenological theory has been developed to explain these successive phase transitions caused by the condensation of the  $M_3$  and  $R_{25}$  zone-boundary phonons. The observed phase-transition schemes can be qualitatively explained by a suitable choice of the parameters in the free-energy expansion with respect to order parameters.

### I. INTRODUCTION

In recent years, extensive investigations have been made on many structural phase transitions. Many cubic perovskite crystals ( $ABX_3$ ) undergo phase transitions in which they transform to slightly distorted structures from the ideal perovskite-type structures. It is well established<sup>1</sup> that these phase transitions are caused by the condensation of the particular normal modes of the phonon in the cubic phase whose eigenvectors correspond to the atomic displacements in the structure stabilized below the transition temperature  $T_c$ . The frequency of this phonon mode decreases as the temperature is lowered to  $T_c$ , and at  $T_c$  the restoring force for this mode vanishes so that the atoms shift to new equilibrium positions.

In some perovskites such as  $\text{BaTiO}_3$ ,  $\text{PbTiO}_3$ , and  $\text{KTaO}_3$ , the transverse-optical mode at the zone center becomes unstable, which explains the occurrence of ferroelectric phase transitions in these substances.<sup>2</sup> On the other hand, the other class of perovskites such as  $\text{SrTiO}_3$ ,<sup>3</sup>  $\text{LaAlO}_3$ ,<sup>4</sup>  $\text{KMnF}_3$ ,<sup>5-7</sup> and  $\text{NaNbO}_3$ <sup>8,9</sup> undergoes phase transitions which are caused by the condensation of the zone-boundary mode associated with the rotation of the  $BX_6$  octahedra. Among these crystals,  $\text{KMnF}_3$  and  $\text{NaNbO}_3$  show successive phase transi-

tions.  $\text{KMnF}_3$  undergoes phase transitions at 184 and 92 K. The transition at 184 K is caused by the condensation of the zone-boundary mode along the [111] direction belonging to irreducible representation  $R_{25}$  of cubic point group  $m\bar{3}m$ . The transition at 92 K is due to the condensation of the zone-boundary mode along the [110] direction belonging to  $M_3$  of point group  $4/m\bar{m}m$ . These both modes represent the rotational vibrations of  $BX_6$  octahedra around cubic principal axes. The difference between the  $R_{25}$  and the  $M_3$  is that the  $R_{25}$  represents the opposite rotation of the neighboring  $BX_6$  octahedra along the rotation axis, whereas the  $M_3$  represents the rotation in the same direction as is illustrated in Fig. 1. In the case of  $\text{NaNbO}_3$ , the  $M_3$  mode first condenses at 640°C and then it is followed by the condensation of the  $R_{25}$  mode at 570°C. This is contrast with the case of  $\text{KMnF}_3$  in which the  $R_{25}$  mode first condenses.

Recently, the perovskite crystal  $\text{CsPbCl}_3$  was found to undergo three successive phase transitions. In 1959, Møller<sup>10</sup> observed the phase transition at 47°C for the first time. He also carried out the structure analysis and reported that the basic structure of this crystal was of perovskite type. In 1969, three groups independently found the other transitions. Sakudo *et al.*<sup>11</sup> observed a broad elastic anomaly at about 40°C. They also

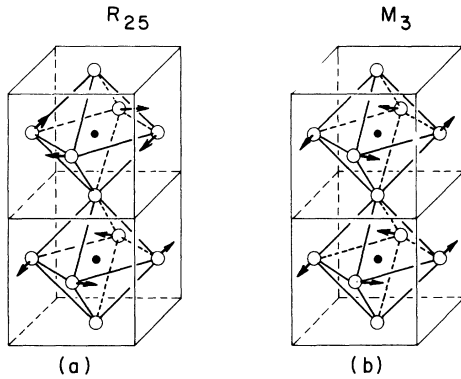


FIG. 1. Displacement patterns of the X ions of cubic perovskite  $ABX_3$  for the modes (a)  $R_{25}$  and (b)  $M_3$ . A ions situated at every corner are omitted for simplicity.

found that superlattice reflections in x-ray-diffraction pattern appear at the X point, the zone boundary along the [001] direction of cubic lattice, at room temperature. Hirotsu and Sawada<sup>12</sup> made optical measurements and confirmed three phase transitions at 47, 42, and 37 °C. Jensen<sup>13</sup> carried out nuclear-quadrupole-resonance (NQR) measurements on the  $Cl^-$  ion using powder specimen and observed three phase transitions in which the transition at 42 °C is of second order and those at 47 and 37 °C are of first order. Hereafter, we designate each phase as follows: phase I ( $T > 47$  °C), phase II ( $47 > T > 42$  °C), phase III ( $42 > T > 37$  °C), and phase IV ( $37 > T$ ). According to his experimental results, the NQR line which is singlet in phase I splits into two lines in phase II. In phase III, the low-frequency line, the intensity of which is about twice as strong as that of the other line, splits into two lines. In phase IV, these two lines become single again as if the Cl site seems to restore a higher symmetry. In 1969, studies of the EPR of  $Mn^{2+}$  doped in  $CsPbCl_3$  were made by Cape *et al.*<sup>14</sup> They discussed the space groups of the crystal at each phase. In 1970 and 1971, Hirotsu<sup>15</sup> made extensive experimental studies including dielectric, elastic, specific-heat, optical, and Raman-scattering measurements. He confirmed that this crystal was not ferroelectric in any phase and also found four temperature-dependent modes by Raman scattering in phase IV. Their frequencies decrease with increasing temperature towards room temperature. However, the mode assignments were not made.<sup>16</sup>

In spite of these extensive experimental works on  $CsPbCl_3$ , the microscopic mechanism of three phase transitions in this crystal has not been elucidated yet. The purpose of the present work is to clarify the mechanism of the structural phase transitions of  $CsPbCl_3$  by neutron-scattering method

and thus to give a general basis to understand successive phase transitions occurring in various perovskite crystals.

This work was presented at the Third International Meeting on Ferroelectricity, Edinburgh, 1973.<sup>17</sup>

## II. EXPERIMENTAL

The earlier part of the present neutron scattering experiments was carried out with the triple-axis neutron spectrometer (ISSP ND-1) installed at the JRR-2 reactor of Japan Atomic Energy Research Institute. The energy of incident neutrons was 14.2 meV from a pyrolytic graphite (002) monochromator. In this case,  $\frac{1}{2}\lambda$  components were eliminated with graphite filters. The germanium (111) plane was used for an analyzer. The collimation angles of four collimators; in-pile, monochromator to sample, sample to analyzer, analyzer to detector, are all 30 min. The constant-Q technique was utilized. The sample crystal has a nearly quadrangular pyramid shape with a 1.2 cm<sup>3</sup> volume and a 15 mm height, and its mosaic spread was measured to be 0.4°. The specimen was set in the electric furnace and the temperature of the specimen was controlled within  $\pm 0.2$ °.

Extensive measurements were also carried out on a triple-axis neutron spectrometer at the High Flux Beam Reactor of Brookhaven National Laboratory. Pyrolytic graphite (002) planes were used for both the monochromator and the analyzer. The inelastic-scattering experiments were carried out

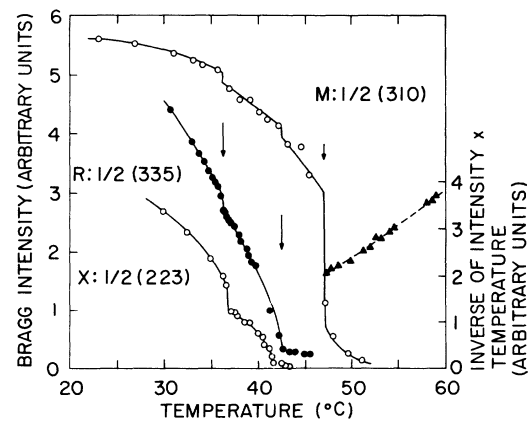


FIG. 2. Temperature dependences of the superlattice reflections observed at the zone boundary points,  $M$ ,  $R$ , and  $X$  along the directions [110], [111], and [001] referred to the cubic lattice, respectively. The arrows indicate the phase transition points. The triangles above 47 °C show the temperature dependence of the temperature times the inverse of the quasielastic scattering intensity observed at the  $M$  point [ $\frac{1}{2}$  (310)].

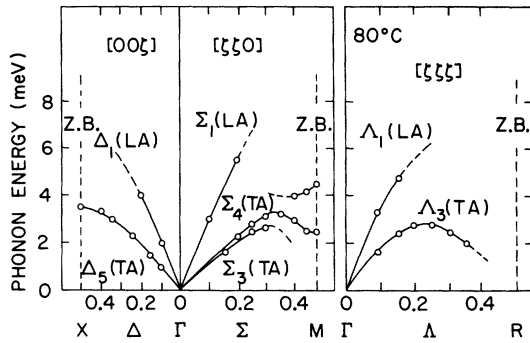


FIG. 3. Phonon dispersion curves along the symmetric directions at 80°C. The parts which are shown by the broken lines were not accurate because of the broadening of the spectra.

with the incident energy of 38 meV and all four collimations were 20 min. On the other hand, most measurements of quasielastic scattering were made with incident energy of 13.7 meV and  $\frac{1}{2}\lambda$  components were eliminated with graphite filters. The in-pile collimation was 20 min and other three collimations were 40 min. The crystal specimen has a nearly triangular pyramid shape with about a 1-cm<sup>3</sup> volume. The temperature of the specimen was kept constant within  $\pm 0.2^\circ$ .

### III. SUCCESSIVE PHASE TRANSITIONS

At room temperature, we observed superlattice Bragg reflections at both zone boundary points  $M$  and  $R$  along the respective directions  $[110]$  and  $[111]$  referred to the cubic lattice. Figure 2 shows the temperature dependences of the intensities of superlattice reflections  $\frac{1}{2}(310)$  and  $\frac{1}{2}(335)$  observed by neutron scattering. The  $\frac{1}{2}(310)$  reflection shows a distinct discontinuity at 47°C and then vanishes above this temperature. The intensity of  $\frac{1}{2}(335)$  reflection gradually decreases with increasing temperature and vanishes at 42°C. It also shows a discontinuity at 37°C. According to the earlier x-ray work by Sakudo *et al.*,<sup>11</sup> the superlattice reflections appear at the  $X$  point, the zone boundary along the  $[001]$  direction, at room temperature. The temperature dependence of its intensity is similar to that of the  $\frac{1}{2}(335)$  reflection as is shown in Fig. 2. These temperature dependences of superlattice reflections clearly show the existence of three phase transitions and that the transition at 42°C would be of the second order and the remaining two are of the first order.

### IV. PHONON DISPERSION

The experimental results in Sec. III suggest that the instabilities of the zone boundary phonons at the points  $M$  and  $R$  as observed in  $\text{KMnF}_3$  and  $\text{NaNbO}_3$

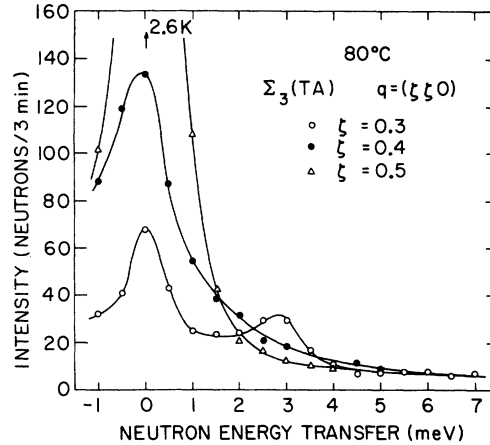


FIG. 4. Energy spectra of scattered neutrons due to  $\Sigma_3(\text{TA})$  phonons at 80°C. In the range of  $\xi > 0.35$ , the phonon becomes overdamped. In the case of  $\xi = 0.3$ , the peak at the zero energy transfer can be explained by the incoherent background. The positive value of the neutron energy transfer corresponds to the energy-loss process of neutrons.

may occur at 47 and 42°C in  $\text{CsPbCl}_3$ , respectively. In order to investigate the behavior of these phonons in the cubic phase, the phonon dispersion curves along the three symmetric directions  $[00\xi]$ ,  $[\xi\xi 0]$  and  $[\xi\xi\xi]$  were measured by neutron-inelastic-scattering method. Figure 3 shows the phonon dispersion curves observed at 80°C (phase I). It is characteristic of the  $\text{CsPbCl}_3$  crystal that the energy of the whole acoustic phonon is remarkably low in comparison with other perovskite crystals such as  $\text{SrTiO}_3$  and  $\text{KMnF}_3$ . Moreover, the phonon branches with the energies larger than about 5 meV are broadened out and become unobserved along any one of three directions. The branches  $\Sigma_3(\text{TA})$  and  $\Delta_3(\text{TA})$  along the directions  $[\xi\xi 0]$  and  $[\xi\xi\xi]$ ,

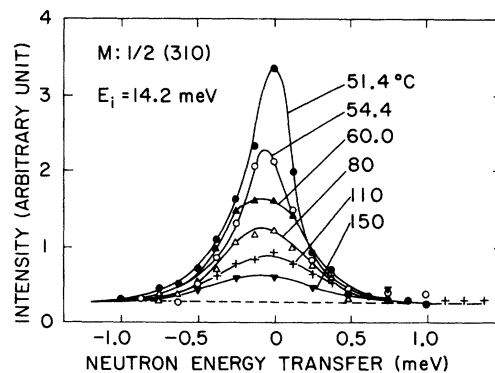


FIG. 5. Temperature dependence of the quasielastic scattering at the  $M$  point  $[\frac{1}{2}(310)]$ . The broken line shows the background. Energy resolution is 0.6 meV FWHM.

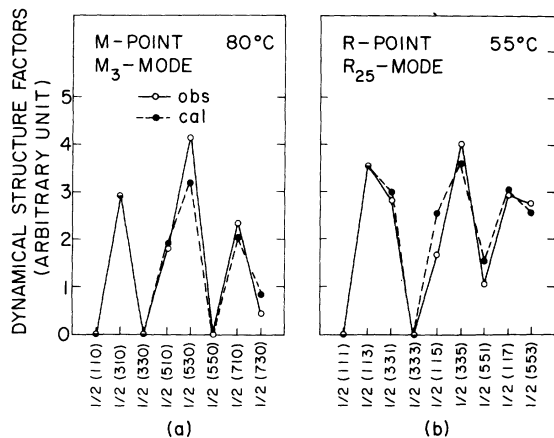


FIG. 6. Comparison between the observed dynamical structure factors (open circles) and the calculated ones (solid circles) at various points in the reciprocal space in phase I. (a)  $M_3$  mode at the  $M$  point and (b)  $R_{25}$  mode at the  $R$  point.

which are compatible with the zone boundary modes  $M_3$  and  $R_{25}$ , respectively, tend to decrease at  $\xi \sim 0.3$  and in the range of  $\xi > 0.35$  they become overdamped. This implies that the condensing modes are  $M_3$  and  $R_{25}$ . In Fig. 4, the energy spectra of the  $\Sigma_3(\text{TA})$  mode along the  $[\xi\xi 0]$  direction are shown. The temperature dependence of the quasielastic scattering due to the overdamped phonon at the  $M$  point  $[\frac{1}{2}(310)]$  is shown in Fig. 5. The energy resolution was 0.6 meV [full width at half-maximum (FWHM)]. The inverse of the intensity of this quasielastic scattering times temperature  $T/I$  is plotted against the temperature  $T$  in Fig. 2. The nearly linear relation between  $T/I$  and  $T$  suggests that the square of the intrinsic undamped phonon frequency  $\omega_0^2$  decreases in proportional to  $T - T_M^*$  as the temperature is lowered to

TABLE I. Crystal system and space group at each phase of  $\text{CsPbCl}_3$ .

Phase I ( $T > 47^\circ\text{C}$ )			
cubic		$O_h^1 - Pm\bar{3}m$	$a \times a \times a$
Pb	1	$a$	$m\bar{3}m$
Cs	1	$b$	$m\bar{3}m$
Cl	3	$d$	$4/m\bar{3}m$
Phase II ( $47 > T > 42^\circ\text{C}$ )			
tetragonal		$D_{4h}^5 - P4/m\bar{2}m$	$\sqrt{2}a \times \sqrt{2}a \times a$
Pb	2	$a$	$4/m$
Cs	2	$c$	$mmm$
Cl-I	2	$b$	$4/m$
Cl-II	4	$g$	$mm$
Cl-III	4	$g$	$mm$
Phase III ( $42 > T > 37^\circ\text{C}$ )			
orthorhombic		$D_{2h}^{17} - Cmc$	$2a \times 2a \times 2a$
Pb	8	$d$	$\bar{1}$
Cs	4	$c$	$mm$
	4	$c'$	$mm$
Cl-I	8	$g$	$m$
Cl-II	8	$f$	$m$
Cl-III	8	$e$	2
Phase IV ( $37^\circ\text{C} > T$ )			
monoclinic		$C_{2h}^2 - P2_1/m$	$\sqrt{2}a \times 2a \times \sqrt{2}a$
Pb	2	$a$	$\bar{1}$
	2	$d$	$\bar{1}$
Cs	2	$e$	$m$
	2	$e'$	$m$
Cl-I	2	$e''$	$m$
	2	$e'''$	$m$
Cl-II	4	$f$	1
Cl-III	4	$f'$	1

the transition temperature  $47^\circ\text{C}$ . Here,  $T_M^*$  is the intrinsic second-order transition temperature. The quasielastic scattering due to the overdamped

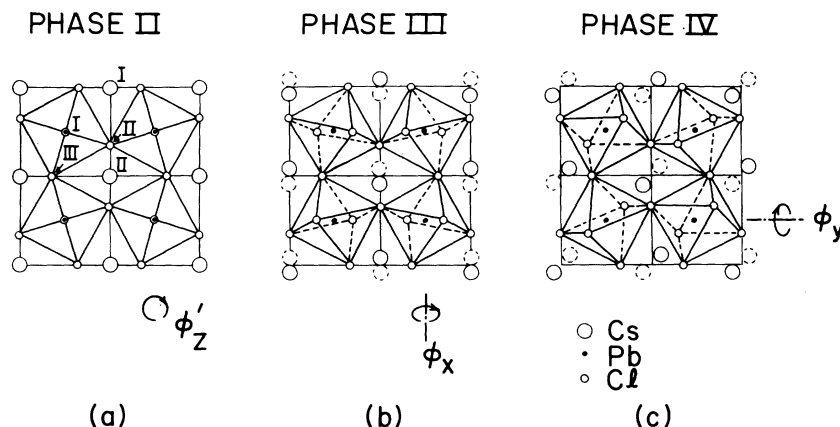


FIG. 7. Crystal structures at (a) phase II, (b) phase III, and (c) phase IV stabilized by the condensation of the modes  $M_3^z$ ,  $Z_3^z$ , and  $Z_3^y$ , respectively. When the Pb ions are taken to be placed on the  $z=0$  plane, the Cs ions drawn with solid and broken circles are placed on the  $z=\frac{1}{4}a$  and  $z=-\frac{1}{4}a$  planes, respectively ( $a$ ; lattice constant of the cubic cell).

phonon at the  $R$  point shows the similar temperature dependence as that at the  $M$  point.

#### V. MODE DETERMINATION AND THE STATIC STRUCTURES

In order to determine the condensing mode of the  $M$  point uniquely, the intensity measurements of the quasi-elastic scattering due to the overdamped phonon were made at the  $M$  points around various reciprocal-lattice points. Figure 6(a) shows the comparison between the observed dynamical structure factors (open circles) and the calculated ones (solid circles) for various  $M$  points at 80 °C. In the calculation, we used the eigenvectors of the  $M_3$  mode illustrated in Fig. 1(b). The temperature factor of the Cl ion determined from the best fitting was  $B_{Cl} = 12.6 \text{ \AA}^2$  at 80 °C. This value corresponds to  $\langle u^2 \rangle = 0.16 \text{ \AA}^2$  in mean-square displacement.

Below 47 °C, the static displacement corresponding to the eigenvector of the  $M_3$  mode takes place. The space group of the static structure at phase II was determined as  $D_{4h}^5 - P4/mbm$  [Fig. 7(a) and Table I]. The directions of the new principal axes of the tetragonal lattice,  $[100]_t$ ,  $[010]_t$ , and  $[001]_t$  are taken along  $[110]$ ,  $[\bar{1}10]$ , and  $[001]$  referred to the pseudocubic lattice, respectively. The unit cell is doubled as compared with the cubic cell. In this phase, the site symmetry of the Cl-I ion is different from that of the ions Cl-II and Cl-III which are placed at the equivalent sites.

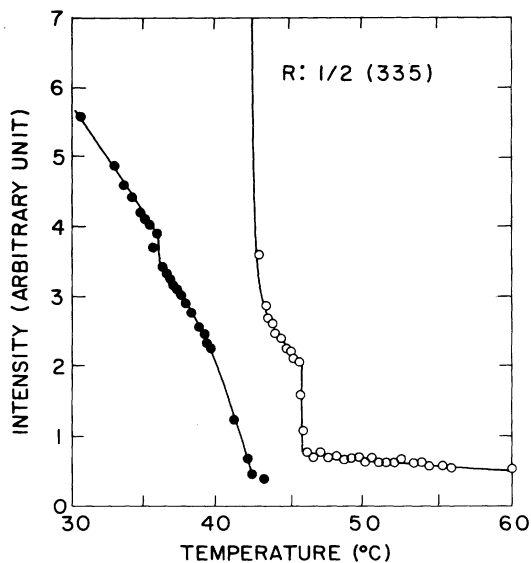


FIG. 8. Temperature dependences of the quasielastic scattering (open circles) and the superlattice Bragg reflection (solid circles) observed at the  $R$  point  $[\frac{1}{2}(335)]$ . The quasielastic scattering increases with decreasing temperature and shows a discrete increase at the cubic-to-tetragonal transition point 47 °C.

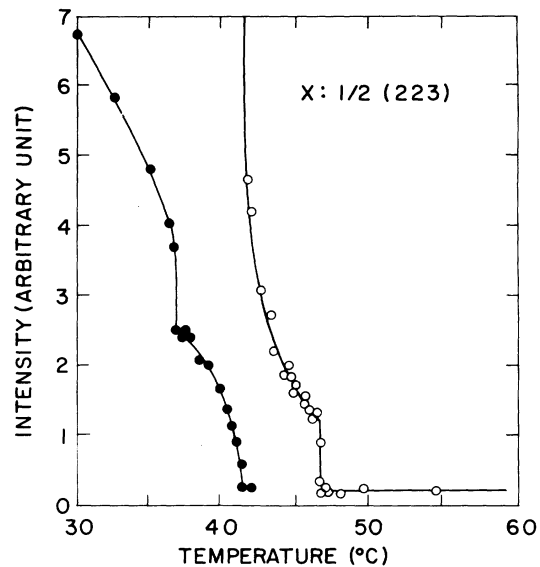


FIG. 9. Temperature dependences of the quasielastic scattering (open circles) and the superlattice Bragg reflection (solid circles) observed at the  $X$  point  $[\frac{1}{2}(223)]$ . The remaining temperature independent intensity above 47 °C is the background, which means that there is no quasielastic scattering above 47 °C at the  $X$  point in contrast with the  $R$  point (cf. Fig. 8).

Following the same procedure as the case of the  $M_3$  mode, observed quasielastic intensities at various  $R$  points were compared with the calculated dynamical structure factors using the eigenvectors of the  $R_{25}$  mode [Fig. 6(b)]. The temperature factor was  $B_{Cl} = 10.5 \text{ \AA}^2$  at this temperature (55 °C). In this case, however, the preceding cubic-to-tetragonal transition at 47 °C causes some complications in exact mode assignments. In Fig. 8, the temperature dependence of the quasi-elastic scattering at  $\frac{1}{2}(335)$  (open circles) is shown together with that of the Bragg reflection at the same point (solid circles). This shows a sudden increase at 47 °C and diverges at 42 °C corresponding to the expected condensation of the  $R_{25}$  mode. The increase at 47 °C is interpreted due to the fact that the triply degenerate  $R_{25}$  mode in the cubic phase splits into a doubly degenerate  $Z_5$  mode and a non-degenerate  $Z_1$  mode in the tetragonal phase as shown later. Another effect of the tetragonality in phase II can be seen in the appearance of quasi-elastic scattering at the  $X$  point referred to the pseudocubic lattice. Figure 9 gives the temperature dependences of the quasielastic scattering and the Bragg reflection at  $\frac{1}{2}(223)$ . Below 47 °C, they show temperature dependences similar to those of the  $R$  point (cf. Fig. 8). This is simply due to the fact that the points  $R$  and  $X$  in the cubic lattice become equivalent in the tetragonal phase, both being

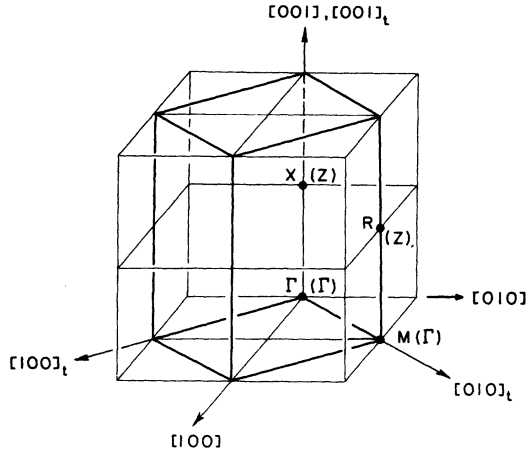


FIG. 10. Relation between the reciprocal lattice of the tetragonal structure stabilized by the condensation of the  $M_3$  mode drawn with the thick lines and that of the cubic structure drawn with the thin lines. The symbols in parentheses are referred to the tetragonal structure and those out of parentheses are referred to the cubic one. The points  $X$  and  $R$  become equivalent in the tetragonal phase, both being  $Z$  points.

the  $Z$  point of the tetragonal cell which is the zone boundary along the tetragonal unique axis as shown in Fig. 10.

In order to investigate how the  $R_{25}$  normal mode at the  $R$  point in the cubic perovskite is modified under the influence of the tetragonality, the normal mode analysis in the tetragonal lattice with the space group  $D_{4h}^5$  was made at the  $Z$  point. The unit cell involves ten ions. At the  $Z$  point, the little group is  $4/mmm$ , and the 30 irreducible representations are obtained as

$$3Z_1 + Z'_1 + 2Z_2 + Z_3 + Z'_3 + 2Z_4 + 2Z'_4 + 5Z_5 + 4Z'_5.$$

Here,  $Z_5$  and  $Z'_5$  correspond to doubly degenerate modes. The doubly degenerate mode representing the rotational vibration of the  $\text{PbCl}_6$  octahedra around the pseudocubic axes  $[100]$  and  $[010]$  belongs to the  $Z_5$  mode. The other nondegenerate rotational mode whose axis of rotation is along the  $[001]$  direction belongs to the  $Z_1$  mode. However, these are not purely rotational mode but are accompanied by the displacements of the other ions. The  $Z_1$  mode is accompanied by the displacements of the both ions Cs and Cl-I along the  $[001]$  direction. The  $Z_5$  mode, on the other hand, is accompanied by the displacement of the Cs ion along the rotation axis of the octahedra. Since the tetragonality is small, one may assume that the condensing mode at the  $Z$  point is either one of these slightly modified  $R_{25}$  type modes. Further the optical measurements<sup>12</sup> have shown that the crystal symmetry in phase III was lower than orthorhombic. There-

fore, the condensing mode is the doubly degenerate mode belonging to  $Z_5$  whose rotation axis is perpendicular to the tetragonal unique axis because the condensation of the  $Z_1$  mode brings only tetragonal symmetry. To specify each of these degenerate modes, let us use the notations  $Z_5^x$  and  $Z_5^y$ , in which the superscripts represent the rotation axis of the  $\text{PbCl}_6$  octahedra. For the  $Z_5^x$  mode, dynamical structure factors at the points  $X$  and  $R$  referred to the pseudocubic lattice are given by

$$\begin{aligned} |F_d^x(X)| \propto & | [b_{\text{Cl}} / (m_{\text{Cl}})^{1/2}] \pi \langle \phi'_x \rangle \phi_x (-1)^l \\ & \times (l + \frac{1}{2}) h e^{-M_{\text{Cl}}} + [b_{\text{Cs}} / (m_{\text{Cs}})^{1/2}] (U_x - U'_x) \\ & \times (-1)^l h e^{-M_{\text{Cs}}} |, \end{aligned} \quad (1)$$

$$\begin{aligned} |F_d^x(R)| \propto & | [b_{\text{Cl}} / (m_{\text{Cl}})^{1/2}] \phi_x [(-1)^{k+l} (k + \frac{1}{2}) \\ & - (l + \frac{1}{2})] e^{-M_{\text{Cl}}} + [b_{\text{Cs}} / (m_{\text{Cs}})^{1/2}] (U_x - U'_x) \\ & \times (-1)^l (h + \frac{1}{2}) e^{-M_{\text{Cs}}} |. \end{aligned} \quad (2)$$

Here  $\phi_x$  represents the rotation angle of the  $\text{PbCl}_6$  octahedra around the  $[100]$  axis.  $\langle \phi'_x \rangle$  is the rotation angle of its octahedra around the  $[001]_t$  axis which plays a role of the order parameter in phase II.  $U_x$  and  $U'_x$  are eigenvectors of the ions Cs-I and Cs-II along the  $[100]$  direction, respectively (see Fig. 7). The indices of the reciprocal lattice points  $h$ ,  $k$ , and  $l$  are referred to the pseudocubic lattice. The similar expressions are obtained as for the  $Z_5^y$  mode. These formula are obtained by the linear expansion of the dynamical structure factor with respect to  $\langle \phi'_x \rangle$ . It is noticed that  $F_d(X)$  is linear to  $\langle \phi'_x \rangle$ , whereas  $F_d(R)$  is independent of  $\langle \phi'_x \rangle$  under the above approximation. In phase I

TABLE II. Comparison between the observed dynamical structure factors and the calculated ones in an arbitrary unit at the points  $R$  and  $X$  referred to the pseudocubic lattice in phase II (45 °C). The observed values are directly comparable between the points  $R$  and  $X$ . The calculation is normalized at two points marked with asterisks.

$R$ point	Obs.	Calc.	$X$ point	Obs.	Calc.
$\frac{1}{2}(111)$	< 0.7	0	$\frac{1}{2}(003)$	< 0.1	0
$\frac{1}{2}(113)$	47.1	47.1*	$\frac{1}{2}(221)$	2.2	0.1
$\frac{1}{2}(331)$	37.7	39.7	$\frac{1}{2}(223)$	13.5	13.5*
$\frac{1}{2}(333)$	< 0.2	0	$\frac{1}{2}(005)$	< 0.6	0
$\frac{1}{2}(115)$	28.6	33.5	$\frac{1}{2}(225)$	10.6	10.6
$\frac{1}{2}(335)$	48.7	47.7	$\frac{1}{2}(441)$	8.0	9.1
$\frac{1}{2}(551)$	15.2	20.1	$\frac{1}{2}(443)$	9.3	9.4
$\frac{1}{2}(117)$	39.0	40.3	$\frac{1}{2}(007)$	< 0.5	0
$\frac{1}{2}(553)$	30.2	34.0	$\frac{1}{2}(227)$	10.9	11.9
			$\frac{1}{2}(445)$	17.2	17.6

in which  $\langle \phi_z' \rangle$  is zero,  $F_d(X)$  vanishes while  $F_d(R)$  has a finite value. This agrees well with the experimental results that no quasielastic scattering is observed at the  $X$  point above 47 °C. The dynamical structure factors obtained from the quasielastic scattering at the points  $X$  and  $R$  measured at 45 °C (phase II) are shown in Table II. In the calculation of the structure factors, Eqs. (1) and (2) are rewritten on the assumption of  $M_{C1} = M_{Cs}$  as

$$|F_d^x(X)| \propto |(-1)^l(l + \frac{1}{2})h + \alpha(-1)^l h| e^{-M_{C1}}, \quad (3)$$

$$|F_d^x(R)| \propto |(-1)^{k+l}(k + \frac{1}{2}) - (l + \frac{1}{2}) + \beta(-1)^l(h + \frac{1}{2})| e^{-M_{C1}}, \quad (4)$$

where  $\alpha$  and  $\beta$  are taken as parameters to be fixed by the best fitting between the observed and calculated intensities. The parameter  $\alpha$  thus obtained is 0.4.  $\beta$  should be smaller than  $\alpha$  by a factor of  $\pi \langle \phi_z' \rangle$  so that the second term of Eq. (4) is negligibly small in comparison with the first term. The same temperature factor of  $B_{C1}$  as obtained at 55 °C was used in this analysis. The calculated dynamical structure factors due to the  $Z_5^x$  mode are shown in Table II. In the calculation, the intensities at the points  $R$  and  $X$  are independently normalized at  $\frac{1}{2}(113)$  and  $\frac{1}{2}(223)$ , respectively. The good agreement between the observed dynamical structure factors and calculated ones confirms that the phase transition at 42 °C is caused by the condensation of the  $Z_5^x$  mode or any linear combination of the modes  $Z_5^x$  and  $Z_5^y$ . In fact, it can be seen that the dynamical structure factors  $F_d^x$  and  $F_d^y$  associated with the respective modes  $Z_5^x$  and  $Z_5^y$  give the same values at the reciprocal-lattice points  $(hkl)$ , where the observation was made. As we see later, however, the condensation of the  $Z_5^x$  mode has been strongly supported by various experimental facts rather than any linear combinations of  $Z_5^x$  and  $Z_5^y$ .

The space group of the proposed crystal structure of phase III attained by this mode condensation was determined to be  $D_{2h}^{17}-Cmcm$  [Fig. 7(b) and Table I]. The directions of the new principal axes of the orthorhombic lattice  $[100]_o$ ,  $[010]_o$ , and  $[001]_o$  are taken along the directions  $[010]$ ,  $[100]$ , and  $[001]$  referred to the pseudocubic lattice, respectively. The unit cell becomes eightfold in comparison with the cubic cell. In this phase, the Cl-I, Cl-II, and Cl-III ions are placed at nonequivalent sites.

As for the phase transition at 37 °C, the same procedure as used to determine the condensing mode at 47 and 42 °C cannot be followed because the quasielastic scattering was masked by the strong Bragg reflection which already exists at  $Z$  point. However, we have observed that the intensities of the Bragg scattering at  $Z$  points observed at 25 °C (phase IV) are nearly proportional to the

intensities of the quasielastic scattering observed at the respective  $Z$  point at 42 °C (phase II). This means that the static structure in phase IV should be also derivable from the condensation of the  $Z_5$  mode. It is reasonable to infer that the phase transition at 37 °C is caused by the condensation of the remaining  $Z_5^y$  mode. Further, as will be discussed in Sec. VI, these two modes,  $Z_5^x$  and  $Z_5^y$ , should have the equal amplitude in the stable low-temperature phase. Thus, the direction of rotation vector of  $\text{PbCl}_6$  octahedra as well as the displacement of Cs ion, will be pointing to the  $[110]$  direction of the pseudocubic lattice in phase IV. Hirotsu and Sawada<sup>12</sup> observed that on cooling the crystal, one of the principal optic axes suddenly rotates from the  $[100]$  direction to  $[110]$  direction at 37 °C transition point. Based on the above consideration, we therefore infer the crystal structure in phase IV as is schematically given in Fig. 7(c). In this structure, the modes  $Z_5^x$  and  $Z_5^y$  condense with equal amplitudes.

The space group is determined as  $C_{2h}^2-P2_1/m$ . The directions of the new principal axes of the monoclinic lattice  $[100]_m$ ,  $[010]_m$ , and  $[001]_m$  are taken along the directions  $[110]$ ,  $[010]$ , and  $[\bar{1}10]$  referred to the pseudocubic lattice. The unit cell is quadrupled in comparison with the cubic cell. The ions Cl-II and Cl-III have very similar ionic arrangements around themselves though they are not crystallographically equivalent.

## VI. PHENOMENOLOGICAL TREATMENT OF SUCCESSIVE PHASE TRANSITIONS

The three successive phase transitions of  $\text{CsPbCl}_3$  show interesting correspondence to the phase transitions of  $\text{BaTiO}_3$ . In the case of  $\text{BaTiO}_3$ , the phase transitions are caused by the condensation of each of triply degenerate optically active modes at the zone center. In the case of  $\text{CsPbCl}_3$ , on the other hand, the phase transitions are caused by successive condensations of the zone boundary modes associated with the rotational vibration of the  $\text{PbCl}_6$  octahedra around the principal axes of the cubic lattice. The amplitudes of the three axial vectors play the role of order parameters in  $\text{CsPbCl}_3$  in contrast with the case of  $\text{BaTiO}_3$ , where three polar vectors (components of the spontaneous polarization) play the same role. Since the substantial part of the atomic displacements in all lower symmetry phases are describable by the eigenvectors of the modes  $M_3$  and  $R_{25}$  in the cubic phase, we may generally express the deviation of the particle density distribution from that in the cubic phase as follows:

$$\delta\rho(r) = \sum_i c_i \psi_i^{(M)}(r) + \sum_i d_i \psi_i^{(R)}(r), \quad i = x, y, z. \quad (5)$$

Here  $\psi_i^{(M)}$  and  $\psi_i^{(R)}$  are the basis functions of the ir-

reducible representations  $M_3$  and  $R_{25}$ . The subscript indicates the axis of rotation.  $\psi_x^{(M)}$ ,  $\psi_y^{(M)}$ , and  $\psi_z^{(M)}$  are nondegenerate eigenvectors at the non-equivalent  $M$  points  $(\frac{1}{2}\frac{1}{2}0)$ ,  $(\frac{1}{2}0\frac{1}{2})$ , and  $(0\frac{1}{2}\frac{1}{2})$  which forms the star of the wave vector in the cubic reciprocal space. On the other hand,  $\psi_x^{(R)}$ ,  $\psi_y^{(R)}$ , and  $\psi_z^{(R)}$  are triply degenerate eigenvectors at the  $R$  point. In this case there are no other independent eigenfunctions since the wave vector  $(\frac{1}{2}\frac{1}{2}\frac{1}{2})$  forms the star by itself. Following Landau's phenomenological theory of the second order phase transition, we expand the free energy of the system in

terms of  $c_i$ 's and  $d_i$ 's up to the sixth order. It is convenient to introduce two order parameters  $\xi$  and  $\eta$  defined by

$$c_i = \xi \gamma_i, \quad d_i = \eta \delta_i, \quad (6)$$

$$\xi^2 = \sum_i c_i^2, \quad \eta^2 = \sum_i d_i^2, \quad (7)$$

$$\sum_i \gamma_i^2 = 1, \quad \sum_i \delta_i^2 = 1. \quad (8)$$

Then the free energy is expressed as follows:

$$\begin{aligned} \delta F(T, \xi, \eta, \gamma_i, \delta_i) = & \frac{1}{2} A (T - T_M^*) \xi^2 + \frac{1}{2} B (T - T_R^*) \eta^2 + \left[ \frac{1}{4} C (\gamma_x^4 + \gamma_y^4 + \gamma_z^4) + \frac{1}{2} D (\gamma_x^2 \gamma_y^2 + \gamma_x^2 \gamma_z^2 + \gamma_y^2 \gamma_z^2) \right] \xi^4 \\ & + \left[ \frac{1}{4} E (\delta_x^4 + \delta_y^4 + \delta_z^4) + \frac{1}{2} F (\delta_y^2 \delta_x^2 + \delta_x^2 \delta_z^2 + \delta_x^2 \delta_y^2) \right] \eta^4 + \left\{ \frac{1}{2} G (\gamma_x^2 \delta_x^2 + \gamma_y^2 \delta_y^2 + \gamma_z^2 \delta_z^2) \right. \\ & + \frac{1}{2} H [\gamma_x^2 (\delta_y^2 + \delta_z^2) + \gamma_y^2 (\delta_x^2 + \delta_z^2) + \gamma_z^2 (\delta_x^2 + \delta_y^2)] \left. \right\} \xi^2 \eta^2 + \frac{1}{8} I (\gamma_x^6 + \gamma_y^6 + \gamma_z^6) \xi^6 \\ & + \left\{ \frac{1}{4} J [\gamma_x^2 (\delta_y^4 + \delta_z^4) + \gamma_y^2 (\delta_x^4 + \delta_z^4) + \gamma_z^2 (\delta_x^4 + \delta_y^4)] + \frac{1}{2} K (\gamma_x^2 \delta_y^2 \delta_z^2 + \gamma_y^2 \delta_x^2 \delta_z^2 + \gamma_z^2 \delta_x^2 \delta_y^2) \right\} \xi^2 \eta^4. \quad (9) \end{aligned}$$

Each term is constructed so that cubic symmetry operations leave it invariant. In the sixth-order terms we have neglected terms which are not essential to explain successive phase transitions. The transition temperatures  $T_M^*$  and  $T_R^*$  are chosen to be the intrinsic second order transition temperatures which are obtained from the extrapolation of  $T/I$  vs temperature (Fig. 2). The equilibrium state at an arbitrary temperature should be determined by the minimization of  $\delta F$  with respect to  $\xi$ ,  $\eta$ ,  $\gamma_i$ 's and  $\delta_i$ 's. At the present stage, one cannot determine the coefficients in Eq. (9) numerically. We investigate only qualitatively the conditions to stabilize the observed four phases.

#### A. Phase I and phase II

In the temperature region sufficiently higher than  $T_M^*$  and  $T_R^*$ , the minimum of the free energy is certainly attained by  $\xi = 0$  and  $\eta = 0$ , that is, by phase I when  $A > 0$  and  $B > 0$  are assumed. Further, as is pointed out in the Sec. V, we have  $T_M^* > T_R^*$ . Therefore, the phase with  $\xi \neq 0$  and  $\eta = 0$  will be first stabilized on cooling from phase I. Further, under conditions that  $C < D < 0$  and  $I > 0$ , the stable phase is attained by  $\gamma_x = \gamma_y = 0$  and  $\gamma_z = 1$ . The deformation in the static structure is expressed by

$$\delta \rho = \xi \psi_z^{(M)}, \quad (10)$$

which represents the observed phase II. The temperature dependence of the order parameter  $\xi$  is given by

$$\xi^2 = (1/2I) \left\{ -C + [C^2 - 4AI(T - T_M^*)]^{1/2} \right\} \quad (11)$$

and the transition temperature  $T_I$  between phases I and II is obtained as

$$T_I = T_M^* + 3C^2/16AI. \quad (12)$$

Corresponding to the first-order transition, the value of  $\xi$  shows a finite jump at  $T_I$  given by  $\xi^2(T_I) = -3C/4I$ .

#### B. Phase III and phase IV

To investigate the lower-temperature phase transitions associated with the condensation of  $Z_5$  mode, we proceed as follows: Let us assume that the order parameter  $\xi$  is not affected very much by the onset of the phase transitions under consideration. In fact, the experimental results show that this assumption is satisfied since the Bragg intensity at the  $M$  point shows little disturbances at the lower two transition points (Fig. 2). On this assumption,  $\xi$  is looked upon as a temperature-dependent parameter, not a thermodynamical variable, whose temperature dependence is simply determined by Eq. (11). This parameter is expressed as  $\langle \xi \rangle$ . The free energy in the tetragonal phase is then given by setting  $\xi = \langle \xi \rangle$ ,  $\gamma_x = \gamma_y = 0$ , and  $\gamma_z = 1$  in Eq. (9):

$$\begin{aligned} \delta F(T, \eta, \delta_i) = & \frac{1}{2} B (T - T_R^*) \eta^2 \\ & + \left[ \frac{1}{4} E' (\delta_x^4 + \delta_y^4) + \frac{1}{2} F' \delta_x^2 \delta_y^2 \right] \eta^4, \quad (13) \end{aligned}$$

with

$$T_R^* = T_R^* - (H/2B) \langle \xi \rangle^2, \quad (14)$$

$$E' = E + J \langle \xi \rangle^2, \quad (15)$$

$$F' = F + K \langle \xi \rangle^2. \quad (16)$$

The stability conditions with respect to  $\delta_i$ 's allow us two sets of solutions depending on the values of  $E'$  and  $F'$ .

1.  $F' > E' > 0$ 

In this case, a solution of  $\delta_x = 1$  and  $\delta_y = 0$  (or  $\delta_x = 0$  and  $\delta_y = 1$ ) gives the minimum of the free energy. The temperature dependence of  $\eta$  is determined by

$$\eta_{\text{III}}^2 = -B(T - T_R^*)/E' . \quad (17)$$

The static structure in this state is given by

$$\delta\rho = \xi\psi_x^{(M)} + \eta_{\text{III}}\psi_x^{(R)} , \quad (18)$$

which corresponds to the observed structure in phase III.

2.  $E' > F'$ 

In this case,  $\delta_x = \delta_y = \pm 1/\sqrt{2}$  gives the stable state. The order parameter  $\eta$  is given by

$$\eta_{\text{IV}}^2 = -B(T - T_R^*)/(E' + F') \quad (19)$$

and the density distribution is

$$\delta\rho = \xi\psi_x^{(M)} + \eta_{\text{IV}}(1/\sqrt{2})(\psi_x^{(R)} + \psi_y^{(R)}) , \quad (20)$$

which corresponds to the structure in phase IV.

It is convenient to map out the stable region of phase III and phase IV with respect to  $E'$  and  $F'$  as is shown in Fig. 11. The state of the system at an arbitrary temperature is represented by the point  $(E', F')$  with  $E' = E + J\langle\xi\rangle^2$  and  $F' = F + K\langle\xi\rangle^2$ . Eliminating  $\langle\xi\rangle^2$ , we obtain

$$F' = (K/J)E' + [F - (K/J)E] . \quad (21)$$

This means that the representative point of the system moves with temperature along the straight line

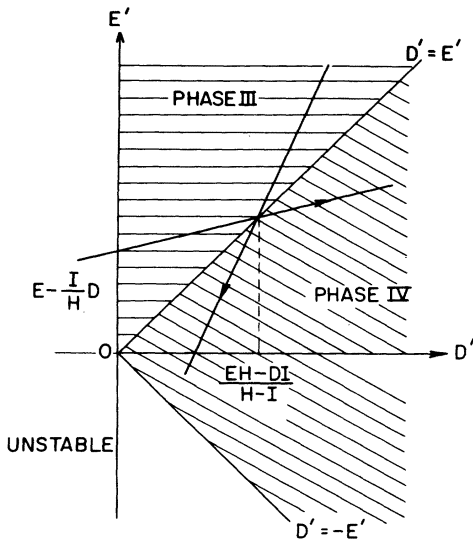


FIG. 11. Stable region of phase III and phase IV with respect to the coefficients  $D'$  and  $E'$ . The arrows represent the trace of the temperature dependence of the system.

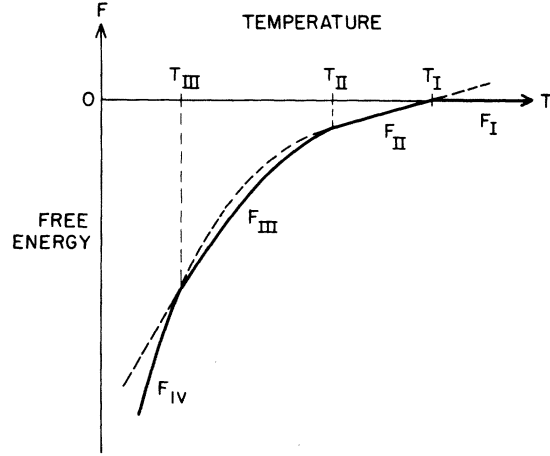


FIG. 12. Schematic diagram of the free energy at each phase.

given by the above formula in the  $E'-F'$  plane. We look for the conditions that the point comes across the boundary in the way that is shown by the arrow in Fig. 11 as the temperature is lowered. The conditions are

$$\begin{aligned} E' < F' & \text{ for } T > T_{\text{III}} , \\ E' = F' & \text{ for } T = T_{\text{III}} , \\ E' > F' & \text{ for } T < T_{\text{III}} . \end{aligned} \quad (22)$$

Here  $T_{\text{III}}$  is the transition temperature between phases III and IV. From the condition (22) together with the assumption that  $\xi$  is monotonically decreasing with increasing temperature, we obtain the following inequalities:

$$F > E > 0 , \quad J > K , \quad FJ > EK . \quad (23)$$

By choosing the coefficients satisfying the equations and inequality conditions given above, the free-energy curves vary with temperature as is schematically shown in Fig. 12. Thus, the observed features of the successive phase transitions of  $\text{CsPbCl}_3$  are qualitatively understood on a phenomenological basis. In order to determine the set of coefficients numerically, more extensive experimental investigations such as determination of the absolute values of order parameters should be carried out.

## VII. DISCUSSION

Since the superlattice reflections at the  $X$  points were observed by Sakudo *et al.*,<sup>11</sup> it has been conjectured that there exists a certain soft zone-boundary mode at the  $X$  point in the cubic phase. However, the present work confirmed that the observed TA phonon at that point is well defined and shows no temperature dependence in the temperature range from 80 to 45 °C. Moreover, the analy-

sis of the quasielastic scattering shows that the overdamped mode at the  $X$  point is associated with the  $Z_5^x$  mode which is derived from the  $R_{25}$  mode. Therefore, the phase transitions of  $\text{CsPbCl}_3$  are simply understood on the common basis of the softening of the rotational modes of  $\text{BX}_6$  octahedra which are characteristic of the perovskite crystal  $\text{ABX}_3$ .

The symmetry properties at each phase determined by the present investigation are comparable with the NQR spectra on  $\text{Cl}^-$  ion measured by Jensen.<sup>13</sup> In phase I, all Cl ions are placed at the equivalent  $3d$  sites shown in Table I, so that they have the same field gradient. This is consistent with the observed single NQR line above 47 °C. In phase II, the ions Cl-II and Cl-III are placed at the equivalent  $4f$  site. On the other hand, the Cl-I ion which does not move by the rotation of the  $\text{PbCl}_6$  octahedra around the  $[001]$  axis, is placed at the  $2b$  site [Fig. 7(a)]. Therefore, two NQR lines must appear in this phase and moreover their intensity ratio is to be 2 : 1, which is consistent with the experimental results. In phase III, the ions Cl-II and Cl-III become crystallographically nonequivalent owing to the rotation of the octahedra around the  $[100]$  axis [Fig. 7(b)]. In this case, it is noted that the Cl-II shifts out of the  $(001)$  plane containing the Pb ions while the Cl-III is placed nearly on its plane, which results in that the environment around the Cl-II is substantially different from that around the Cl-III. Then, the stronger NQR line in phase II should split into two lines with nearly equal intensities. This explains the observed triple lines in phase III. In phase IV, the Cl-III also shifts out of the original  $(001)$  plane while the Cl-II stays at nearly the same position as in phase III [Fig. 7(c)]. The ionic arrangement around the Cl-II is found to be very similar to that around the Cl-III, although their sites are crystallographically nonequivalent. Therefore, two lines which once split in phase III may come close together in phase IV. These two adjacent NQR lines may be observed as a single line if their splitting is within the resolution of the spectrometer. This situation is visualized more clearly by the following considerations. If we assume that at phase II the rotation of the  $\text{PbCl}_6$  octahedra around the  $[001]$  axis is infinitesimally small, the space group of the structure stabilized by the condensation of the  $Z_5^x$  mode is  $D_{2h}^{23}$ . In this case, the Cl-II and Cl-III are placed at nonequivalent sites ( $8f$  and  $8h$ ). On the other hand, the condensation of  $Z_5^x + Z_5^y$  mode gives the structure with the space group  $D_{2h}^{28}$ . In this structure, the both ions Cl-II and Cl-III are placed at the equivalent  $8g$  site. Therefore, when the rotation angle of the  $\text{PbCl}_6$  octahedra caused by the condensation of the  $M_3$  mode is small, the ions Cl-II and Cl-III in phase IV may be regarded as nearly equivalent.

The successive phase transitions of  $\text{CsPbCl}_3$  essentially originate from two different mechanisms. The one is that the condensing  $R_{25}$  mode is degenerate in the higher symmetry phase. In this case, the transition are interpreted on the same line as the successive phase transitions of  $\text{BaTiO}_3$ . The other is that the  $M_3$  mode and the  $R_{25}$  mode have nearly equal frequencies and show similar temperature dependences. From a microscopic standpoint, we can understand the major reason for these facts as follows: In the frame work of the rigid ion model, the characteristic frequencies of the  $T_2$  phonon branch along the  $[\frac{1}{2}\frac{1}{2}\zeta]$  direction which is compatible with the modes  $M_3$  and  $R_{25}$  at  $\zeta=0$  and  $\zeta=0.5$ , respectively, is given by

$$\omega^2(T_2) = (1/m_X) \{A_1 + B_1 + B_2 + 4B_3 + (Z_X^2 e^2/v)[C_1(\zeta) - C_2(\zeta)]\}. \quad (24)$$

Here, we have used the same notations for various short-range force constants as Cowley used in his paper.<sup>18</sup> The electrostatic part  $C_1(\zeta) - C_2(\zeta)$  calculated with Ewald's method shows little  $\zeta$ -dependence along the  $[\frac{1}{2}\frac{1}{2}\zeta]$  direction. For  $\text{CsPbCl}_3$ , the difference  $\omega^2(M_3) - \omega^2(R_{25})$  is calculated to be 0.8 meV.<sup>2</sup> This implies nearly flat dispersion of the  $T_2$  branch of  $\text{CsPbCl}_3$  as is observed in  $\text{KMnF}_3$ .<sup>19</sup> In fact, the remarkable anisotropic quasielastic scattering which extends from the  $M$  point  $[\frac{1}{2}(310)]$  to the  $R$  point  $[\frac{1}{2}(311)]$  was observed in the present experiment. We should note that in Cowley's calculation of phonon dispersion curves of  $\text{SrTiO}_3$ ,<sup>18</sup> the frequencies of both modes  $M_3$  and  $R_{25}$  are imaginary, which suggests the characteristics of perovskite crystals.

It is noted that the soft modes in this crystal are heavily overdamped and moreover the higher-frequency phonons with energy  $\omega > 5$  meV are not observable because of the broadening of the spectra. These results suggest that the anharmonicity of the potential will be extremely large in the cubic phase. In connection with this, it is noticeable that the observed Debye-Waller factors in the cubic phase give extraordinary values. The mean square displacement of Cl ions at 80 °C is  $0.16 \text{ \AA}^2$ , which is about one order of magnitude larger than that of the usual ionic crystal. Møller,<sup>10</sup> in his structure analysis in the cubic phase, suggested that there is disordered arrangement of ions in which Cl ions and Cs ions take several equivalent positions slightly displaced from the ideal perovskite positions. On the other hand, the observed small transition entropy ( $0.25 \text{ cal mole}^{-1} \text{ K}^{-1}$ , Ref. 15) associated with the 47 °C phase transition suggests that even if the averaged structure is disordered, the motions of Cl ions are not independent but they move collectively so that the framework of the  $\text{PbCl}_6$  octahedra remains rigid.

## ACKNOWLEDGMENTS

This work is supported in part by U. S. -Japan Cooperative Science Program performed by U. S. National Science Foundation and Japan Society for Promotion of Science. We would like to thank S.

Hirotsu for providing good single crystals and J. Harada for sending us his x-ray data prior to publication and for his valuable discussion. Stimulating discussions with J. D. Axe, G. Honjo, V. J. Minkiewicz, H. Motegi, K. Uchino, and K. Yagi are acknowledged.

\*Now on leave at Brookhaven National Laboratory.

†Work supported in part by U. S. -Japan Cooperative Science Program.

‡Work performed under the auspices of the U. S. Atomic Energy Commission.

<sup>1</sup>W. Cochran, *Adv. Phys.* **9**, 387 (1960); **18**, 157 (1969).

<sup>2</sup>See, for example, G. Shirane, *Structural Phase Transitions and Soft Modes*, edited by E. J. Samuelson *et al.* (Universitetsforlaget, Oslo, 1971), p. 217.

<sup>3</sup>G. Shirane and Y. Yamada, *Phys. Rev.* **177**, 858 (1969).

<sup>4</sup>J. D. Axe, G. Shirane, and K. A. Müller, *Phys. Rev.* **183**, 1256 (1969).

<sup>5</sup>V. J. Minkiewicz and G. Shirane, *J. Phys. Soc. Jap.* **26**, 674 (1969).

<sup>6</sup>G. Shirane, V. J. Minkiewicz, and A. Linz, *Solid State Commun.* **8**, 1941 (1970).

<sup>7</sup>V. J. Minkiewicz, Y. Fujii, and Y. Yamada, *J. Phys. Soc. Jap.* **28**, 443 (1970).

<sup>8</sup>F. Dénoyer, R. Cômes, and M. Lambert, *Solid State Commun.* **8**, 1979 (1970); *Acta Crystallogr. A* **27**, 414 (1971).

<sup>9</sup>K. Ishida and G. Honjo, *J. Phys. Soc. Jap.* **34**, 1279 (1973).

<sup>10</sup>C. K. Møller, *Mat. Fys. Medd. Danske Vidensk*

*Selsk.* **32**, No. 2 (1959).

<sup>11</sup>T. Sakudo, H. Unoki, Y. Fujii, J. Kobayashi, and M. Yamada, *Phys. Lett. A* **28**, 542 (1969).

<sup>12</sup>S. Hirotsu and S. Sawada, *Phys. Lett. A* **28**, 762 (1969).

<sup>13</sup>N. Torberg-Jensen, *J. Chem. Phys.* **50**, 559 (1969).

<sup>14</sup>J. A. Cape, R. L. White, and R. S. Feigelson, *J. Appl. Phys.* **40**, 5001 (1969).

<sup>15</sup>S. Hirotsu, *J. Phys. Soc. Jap.* **28S**, 185 (1970); **31**, 552 (1971).

<sup>16</sup>Recently, x-ray- and electron-diffraction experiments of this crystal have been made by H. Ohta, J. Harada and S. Hirotsu, *Solid State Commun.* (to be published) and by K. Uchino, K. Yagi, and G. Honjo (private communications), respectively. It has been reported that the phase transitions at 47 and 42°C are caused by the condensation of the respective zone boundary modes  $M_3$  and  $R_{25}$ , which agrees with the result of the present work independently carried out.

<sup>17</sup>Y. Yamada, Y. Fujii, S. Hoshino, J. D. Axe, and G. Shirane, *Ferroelectrics* (to be published).

<sup>18</sup>R. A. Cowley, *Phys. Rev.* **134**, 981 (1964).

<sup>19</sup>K. Gesi, J. D. Axe, G. Shirane, and A. Linz, *Phys. Rev. B* **5**, 1933 (1972).